Angle-resolved photoemission study of the valence-band structure of $VN_{0.89}(100)$

J. Lindström, P. A. P. Lindberg, and L. I. Johansson
Department of Physics and Measurement Technology, Linköping University, S-581 83 Linköping, Sweden

D. S. L. Law
Science and Engineering Research Council, Daresbury Laboratory, Daresbury, Warrington WA4 4AD, United Kingdom

A. N. Christensen
Department of Chemistry, Aarhus University, DK-8000 Aarhus C, Denmark
(Received 3 June 1987)

The electronic structure of a $VN_{0.89}(100)$ single crystal has been studied using angle-resolved photoemission spectroscopy and synchrotron radiation. Recorded normal-emission spectra are compared with theoretical photoemission spectra calculated for stoichiometric composition. A good overall agreement between recorded and calculated spectra is found for photon energies below about 35 eV. A mapping of the band structure is made and compared with a theoretical bulk-band structure. The experimentally determined dispersions of the energy bands are found to be smaller than those theoretically predicted and the location of the bands deviates, in some cases considerably. A vacancy-induced structure is identified at 2.8 eV below the Fermi energy in spectra recorded at photon energies above 31 eV. The character of the vacancy-induced states and of states located close to the Fermi energy is discussed based on observed intensity enhancements above the V $3p$ absorption threshold.

INTRODUCTION

Vanadium nitride, VN, has properties which are of considerable physical and technological interest.[1,2] It is refractory, extremely hard, and has metallic conductivity. It crystallizes in a stable sodium chloride structure over a wide range of compositions, but rarely exists in stoichiometric composition. Vacancies are distributed on the nonmetal sites in the lattice and their presence strongly affects the properties of the compound. The transition temperature for superconductivity, for instance, is reported[3] to decrease strongly with increasing vacancy concentration. Since many of the macroscopic properties are determined by the distribution of valence-band electrons, a detailed experimental investigation of the electronic structure is of fundamental interest. We have performed such an investigation for the purpose of studying the bulk-band structure and how the presence of vacancies may affect the electronic structure. Detailed theoretical studies of the electronic structure of stoichiometric[4,5] and substoichiometric[6,7] VN have been reported previously, but earlier experimental studies[5,8] of VN have been limited. A detailed experimental investigation of the electronic structure of VN was therefore motivated.

In the present study synchrotron radiation has been utilized in angle-resolved photoemission experiments carried out on a $VN_{0.89}(100)$ single crystal. Normal-electron-emission spectra recorded using photon energies in the range 17–60 eV are presented below and compared with theoretical spectra calculated for stoichiometric composition. The theoretical spectra were calculated using the potential generated in an earlier band-structure calculation.[4,5] The overall agreement between calculated and experimental spectra is quite good, especially for photon energies below about 35 eV. At lower photon energies, it is evident from a comparison between experimental and theoretical results that most of the observed structures originate from direct bulk-band transitions. The recorded normal-emission data allow a detailed comparison of experimental and calculated bulk-band dispersions to be made along the $\Gamma-X$ direction.

At higher photon energies, however, additional structures appear which cannot be explained by the calculated results for stoichiometric composition. In the spectra recorded at photon energies above 31 eV, a peak is observed at 2.8 eV below the Fermi level. This peak is interpreted as originating from vacancy-induced states, in accordance with recent theoretical density-of-states calculations[6,7] of substoichiometric VN, which revealed a vacancy-induced structure at about -2.4 eV.

A strong resonance enhancement of the electron emission from states located just below the Fermi level is observed at photon energies between about 35 and 60 eV. Intensity modulations, although weaker, are also observed for the vacancy-induced states in this photon energy range. These intensity modulations with photon energy are investigated and their origin is discussed below.

EXPERIMENTAL DETAILS

The angle-resolved photoemission experiments were carried out at beam line 6.2 at Daresbury Laboratory. The beam line is equipped with a toroidal grating monochromator and an angle-resolved VG ADES 400 electron spectrometer, operating at a base pressure of less than 1×10^{-10} Torr. The energy resolution of the monochromator and the analyzer were both selected to be better than 0.2 eV, giving a total energy resolution of about 0.3 eV. The acceptance angle of the electron analyzer was $\pm2°$. A tungsten grid, located behind the exit slit of the monochromator, allowed for photon-flux normalization.

The VN single crystal was made by zone-melting crystal growth of a polycrystalline rod of VN, and afterwards annealed in high pressure of very pure nitrogen.[9] The bulk composition of the crystal has been found to be $VN_{0.89}$, and it thus contains vacancies in the nonmetal sublattice. The crystal was cleaned *in situ* by repeated flash heatings to about 1100 °C. This cleaning procedure produced a clean and well-ordered (100) surface, as checked by low-energy electron diffraction (LEED) and photoemission. The surface was stable; no change in the LEED pattern or in the photoemission spectra could be observed after repeated flash heatings. A previous investigation[10] of the surface stoichiometry on TiC(100) using angle-resolved photoemission and ion-scattering experiments could not detect any concentration gradient after flash heatings to about 1500 °C. In this investigation the surface and the bulk are assumed to have the same stoichiometry. Using LEED the (100) surface was oriented perpendicular to the analyzer plane within $\pm1°$ and the $\langle010\rangle$ azimuth was oriented to be parallel to the analyzer plane, i.e., with the radiation incident along that azimuth. The radiation was polarized with the main part of the electric-field vector in the analyzer plane. The incidence angle of the photons θ_i is given relative to the surface normal and the energy is referenced to the Fermi energy. All the energy distribution curves (EDC's) presented below were recorded at normal electron emission, thus probing the Δ bands along the $\Gamma-X$ direction.

CALCULATED SPECTRA

Angle-resolved photoemission spectra have been calculated using an extended version,[11] applicable to binary compounds, of the time-reversed LEED scheme.[12] The calculations were made for the stoichiometric composition, $VN_{1.0}$, of the (100) surface. The bulk potentials within the muffin-tin spheres were taken from a previous linear augmented-plane-wave (LAPW) band-structure calculation.[4] In order to simulate bulklike photoemission spectra, the bulk potential and atomic positions were used in all layers. The surface barrier was located to touch the muffin-tin spheres of the largest atoms in the surface layer and its height was determined from the work function. The lifetime broadening parameters for the low- and high-energy electron states were chosen to be -0.14 eV and -2.0 eV, in accordance with earlier calculations[13,14] on transition-metal carbides and nitrides (TMCN's). Thus there has been no attempt to optimize the spectra solely for VN to get a better resemblance to experimental spectra. The polarization vector of the incident radiation was chosen to lie in the analyzer plane, assuming linearly polarized radiation. No corrections for reflection or refraction at the surface have been done in the calculations and hence only relative intensities within each photoemission spectrum should be compared. Furthermore, the calculations assume ideal monochromatic radiation, a perfect smooth crystal surface, and a vanishingly narrow acceptance angle of the analyzer. This cannot be realized in an experimental situation. The energies in the calculated spectra are given relative to the Fermi energy (E_F).

RESULTS

The valence-band structure of VN consists of hybridized V 3*d* and N 2*p* states, distributed between the Fermi energy and about 9 eV binding energy, as illustrated in the wide-scan spectrum in Fig. 1. Below the valence-band structure a weak peak originating from N 2*s* states is observed around 18 eV and a V 3*p* peak is seen at ap-

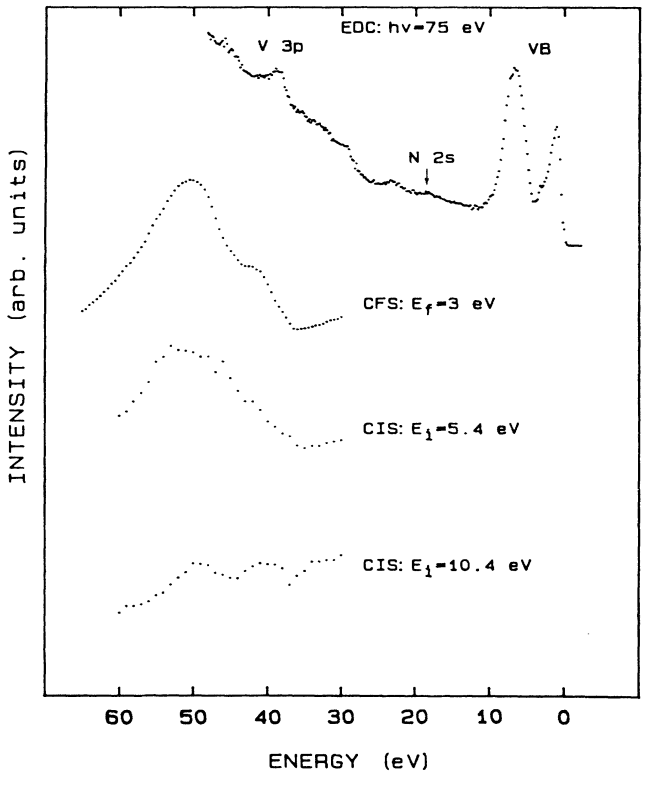

FIG. 1. Normal-emission EDC of $VN_{0.89}$(100) recorded at 75-eV photon energy and at $\theta_i=45°$. The inserted CFS spectrum was recorded at a final-state energy (E_f) of 3 eV and the two CIS spectra at initial-state energies (E_i) of 5.4 and 10.4 eV, respectively. The energy scale is binding energy for the EDC and photon energy for the CFS and CIS spectra. The final- and initial-state energies E_f and E_i are referenced to the vacuum level.

proximately 39 eV. Inserted in Fig. 1 is a constant-final-state (CFS) spectrum and two constant-initial-state (CIS) spectra, measured at photon energies between 30 and 60 eV. In the CFS and the CIS spectra the final and the initial state energies are given with respect to the vacuum level. The electron yield from a tungsten-grid beam monitor was used as a reference counter in these measurements and the spectra have been corrected for variations in the absorption coefficient of the tungsten grid.[15] The CIS spectra were measured with the initial states at 5.4 and 10.4 eV, i.e., the initial-state energies of the two strong valence-band structures in the wide scan spectrum. In a CIS measurement the photon energy and the kinetic energy of the detected electrons are scanned simultaneously, and thus the spectrum reflects the variation in emission intensity from the selected initial states. The resulting CIS curve, for the initial states at 5.4 eV, shows a broad but pronounced intensity enhancement with a maximum at about 53 eV, while the CIS spectrum, for the initial states at 10.4 eV, essentially shows a slow decrease in intensity with increasing photon energy. In the CFS measurement the photon energy is scanned while inelastically scattered electrons of a fixed kinetic energy are detected, and therefore the spectrum reflects the absorption of photons as a function of photon energy. The CFS spectrum, in Fig. 1, shows the broad absorption resonance expected for V $3p \rightarrow 3d$ absorption processes.[16–18] The similarity in shape and maximum locations of the CIS spectrum recorded at an initial state energy of 5.4 eV and the CFS spectrum strongly suggests that the resonance enhancement in intensity of states just below the Fermi energy is related to photon absorption processes. The resonance is interpreted as originating from V $3p \rightarrow 3d$ excitations followed by super Coster-Kronig decay;

$$3p^6 3d^3 + h\nu \rightarrow 3p^5 3d^4 \rightarrow 3p^6 3d^2 + e^- \ .$$

Such photoemission resonances have previously been identified on ZrN, TiN, and NbC,[19–22] and they all showed a resonance maximum about 10 eV above the metal $3p$ ($4p$) threshold. The absorption resonance maximum in VN is approximately 11 eV above the V $3p$ absorption threshold, in conformity with these earlier results. The resonance emission contributes to the intensity in the photoemission spectra, and will thus interfere with the contribution from direct bulk-band transitions and make the interpretation of the experimental results more complicated.

Angle-resolved photoemission spectra from $VN_{0.89}(100)$ recorded at normal electron emission using photon energies between 17 and 60 eV are shown in Figs. 2–5(a). Several prominent structures appear in the spectra and are labeled from A to E. The main symmetry character of the initial states, from which these structures originate, can be determined from their relative variation in intensity when changing the angle of incidence, θ_i. At normal electron emission, symmetry selection rules[23] show that the radiation component parallel to the surface can excite only initial states of Δ_5 symmetry and the component perpendicular to the surface only initial states of Δ_1 symmetry. Thus the relative intensity ratio between peaks of Δ_5 and Δ_1 symmetry will decrease with increasing θ_i. The observed relative peak intensity in the spectra measured at θ_i equal to 45° and 18° [see Figs. 2(a) and 3(a)] show that peaks B and D have Δ_5 and peak E has Δ_1 symmetry. These symmetry assignments of peaks D and E agree with earlier experimental findings.[5]

The calculated angle-resolved photoemission spectra for photon energies below 35 eV, shown in Figs. 2(b) and 3(b), also allow the origin of structures A, B, D, and E in the corresponding experimental spectra to be identified. At energies between 25 and 29 eV, two dominant structures are observed in the spectra calculated at θ_i equal to 18°; see Fig. 3(b). The polarization dependence of these structures shows that they originate from initial states of Δ_5 symmetry. At these energies the calculated spectra predict emission from Δ_1 initial states close to the Fermi energy, which should thus contribute to peak A in the experimental spectra. The deepest-lying structure in the experimental spectra, peak E, is at the lower energies well reflected by the calculated curves, with a polarization dependence showing that it originates from Δ_1 initial states. Above 25 eV, however, this structure appears much stronger in the experimental curves than in the calculated spectra, which show the emission from this Δ_1 band to be smeared out over several eV. This arises because the initial- and final-state bands involved are, at these photon energies, almost parallel, and since they have a large slope it results in a large peak width and an apparent loss in intensity.[24] At these energies, peaks E in the experimental spectra seem to reflect strong band-edge emission instead of direct transitions. Apart from this discrepancy concerning peak E at the

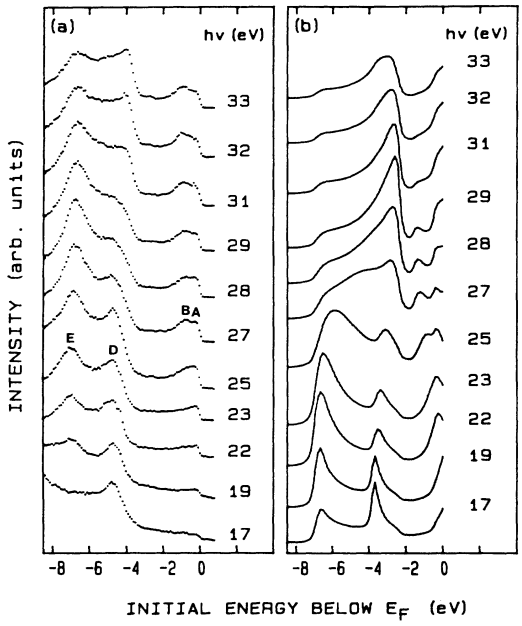

FIG. 2. Normal-emission EDC's for photon energies between 17 and 33 eV, and at $\theta_i = 45°$. (a) Experimental spectra for $VN_{0.89}(100)$. (b) Calculated spectra for $VN_{1.0}(100)$.

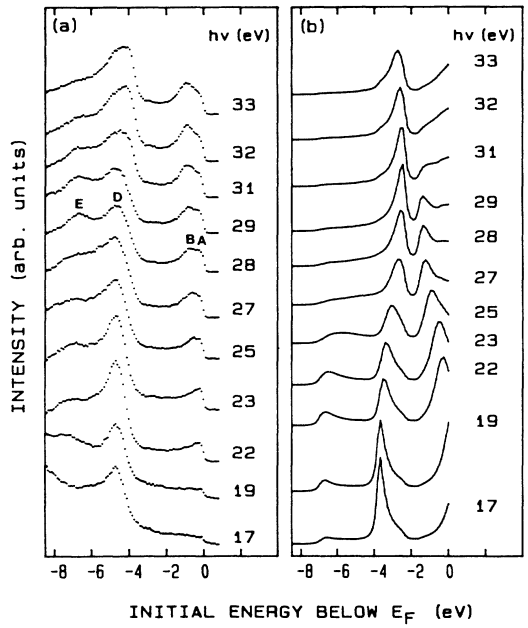

FIG. 3. Normal-emission EDC's for photon energies between 17 and 33 eV, and at $\theta_i = 18°$. (a) Experimental spectra for $VN_{0.89}(100)$. (b) Calculated spectra for $VN_{1.0}(100)$.

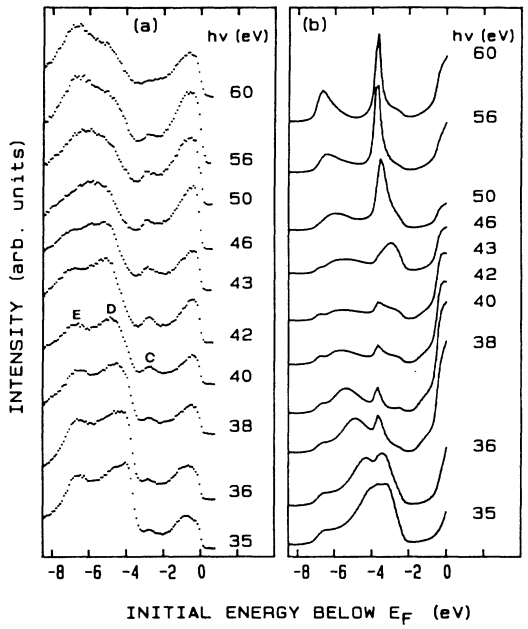

FIG. 4. Normal-emission EDC's for photon energies between 35 and 60 eV, and at $\theta_i = 45°$. (a) Experimental spectra for $VN_{0.89}(100)$. (b) Calculated spectra for $VN_{1.0}(100)$.

higher photon energies, the theoretical spectra shown in Figs. 2(b) and 3(b) are seen to explain the origin and appearance of most of the features observed in the experimental spectra. The actual peak locations deviate however considerably especially for the Δ_5 derived features. This point is illustrated and discussed in detail below.

At higher photon energies larger differences between calculated and experimental spectra are found as illustrated in Figs. 4 and 5, where spectra calculated between 35 and 60 eV are shown. At the highest energies structures *D* and *E* overlap quite strongly in the experimental spectra, while the calculated curves show a separation between these Δ_5- and Δ_1-derived features similar to that obtained around 20 eV. The calculated spectra indicate strong contribution from Δ_1 derived state close to the Fermi energy at photon energies between 38 and 43 eV, which is not observed in the experimental spectra. A major difference between the calculated and experimental results is the appearance of peak *C* in the experimental spectra, exhibiting a Δ_1 polarization dependence. No such Δ_1 derived feature located between the structure at the Fermi energy and the main Δ_5 derived peak is observed in the calculated curves. An interpretation of the origin of this peak is discussed below. At the lowest photon energies shown in Figs. 4 and 5 the calculated curve resemble quite well the experimental curves, if peak *E* is assigned to strong band-edge emission. At photon energies above the V 3*p* absorption threshold larger differences between experimental and theoretical spectra are expected since resonance photoemission effects, which are not accounted for in the theoretical model used, give a significant contribution to the photocurrent. We believe this to be the main reason for the discrepancies observed although other effects may also contribute.[19,20]

The recorded normal emission spectra allow, by assuming direct transitions and utilizing the LAPW band-structure calculation,[4,5] a direct mapping of the initial-state band structure along the Γ—X symmetry direc-

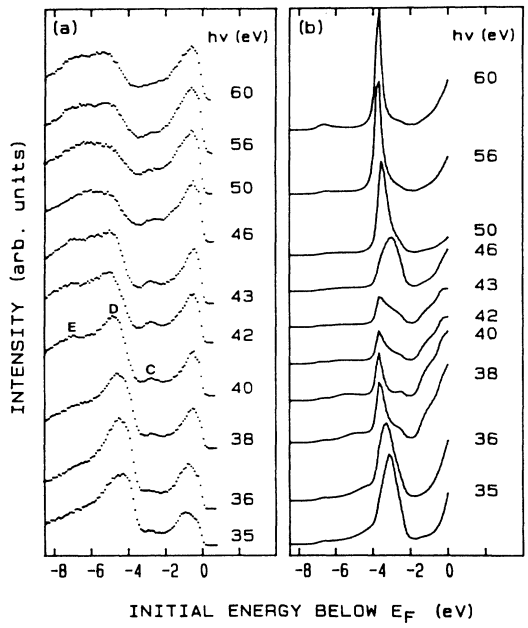

FIG. 5. Normal-emission EDC's for photon energies between 35 and 60 eV, and at $\theta_i = 18°$. (a) Experimental spectra for $VN_{0.89}(100)$. (b) Calculated spectra for $VN_{1.0}(100)$.

tion. At high photon energies, however, the previously discussed resonance effects contribute so much to the photoemission spectra that we selected to use only spectra recorded at photon energies of less than 35 eV. Even so, the band mapping did produce artificial splittings of the Δ_5 bands close to the Γ point when the calculated final state Δ_1 bands were utilized. The energy extrema of the Δ_5 bands did not appear close to the Γ point, which they certainly should in this case. The reason for these effects we believe is due to the fact that the calculated final-state band structures exhibit band gaps and fairly flat bands above 30 eV (and also around 10 eV), as illustrated in Fig. 6. We therefore instead tried fitted free-electron bands and found that when using a band with an effective mass of $m^* = 1.13 m_0$ (dashed line in Fig. 6) the energy extrema of the experimentally determined Δ_5 bands appear close to the Γ point and that no splitting appears. This is the main reason why for the band mapping we used this fitted free-electron band instead of the calculated Δ_1 final-state bands. The result of the band mapping along the Γ–X direction is shown in Fig. 7 together with the calculated band structure. Solid circles represent the experimentally determined energy locations of peaks *B*, *D*, and *E*, i.e., of the Δ_5 and Δ_1 bulk bands. Triangles represent the location of peak *C*, and open circles the energy position of peak *A*. The bandwidths (the total dispersion) of the experimental bands are smaller than those calculated. The two experimentally determined Δ_5 bands are at the $\Gamma_{25'}$ and Γ_{15} points, located respectively about 0.55 eV above and 1.95 eV below the corresponding calculated bands.

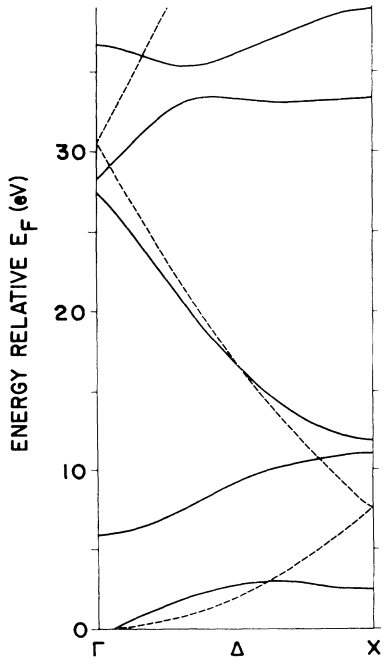

FIG. 6. The calculated LAPW Δ_1 final-state band structure (——) and the fitted free-electron band (— — —) used in the band mapping, with an effective mass $m^* = 1.13 m_0$.

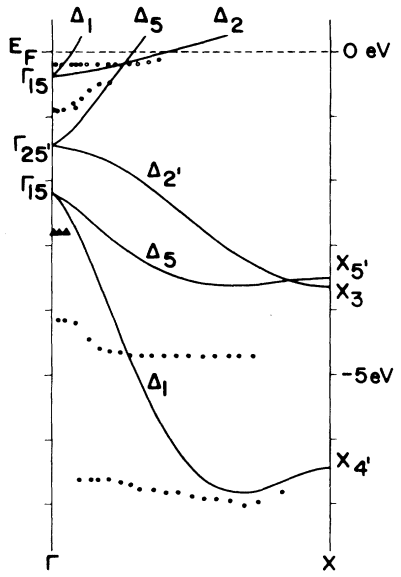

FIG. 7. Comparison between the experimental and calculated initial-state band structure. The solid circles (●) represent peaks interpreted as originating from Δ_1 and Δ_5 initial states, triangles (▲) from vacancy-induced states, and the open circles (○) are mainly DOS effects.

However, the minimum of the experimental Δ_1 band agrees well with the calculated minimum, only about 0.12 eV below. The steep part of the Δ_1 band was not possible to map out for reasons discussed above, a difficulty observed also in earlier studies[19,21,25] of TMCN's. The quite large discrepancy between the position of the experimental and calculated Δ_5 band at lower binding energy (peak *D*) could partly be explained by vacancy interactions. Recent calculations[26,27] for $ZrN_x(100)$ and $TiN_x(100)$ have shown that the introduction of vacancies affects this Δ_5 band more than the deeper lying Δ_1 band and actually pushes the Δ_5 band to a lower energy position.

The location of peak *C* at about -2.8 eV is represented by triangles in Fig. 7. This peak appears in the spectra at photon energies above 31 eV and it has not counterpart in the theoretical spectra; see Figs. 2–5. It cannot originate from the $\Delta_{2'}$ initial band, because it shows little or no dispersion and the polarization dependence is characteristic for states of Δ_1 symmetry; compare Figs. 4(a) and 5(a). At normal electron emission, transitions from the $\Delta_{2'}$ band are moreover forbidden by symmetry selection rules. Peak *C* is instead interpretated as originating from vacancy-induced states. This interpretation is consistent with the results of recent calculations[6,7] of substoichiometric VN which showed a vacancy-induced structure at about -2.4 eV, i.e., in the minimum of the density of states (DOS) of the stoichiometric compound. A "Δ_1-like" behavior of vacancy-induced states has been observed earlier in angle-resolved studies[19,21] of ZrN, TiN, and NbC, and recent theoretical results[26–29] also predict this polarization dependence of vacancy states in

these compounds. This vacancy-related structure was not observed in earlier photoemission studies[5,8] of substoichiometric VN. However, the fact that it does not appear in our normal emission spectra at photon energies below 32 eV explains why it was not observed in the previous studies where 16.8- and 21.2-eV radiation was used. Calculated photoemission spectra for $TiN_{0.83}(100)$ (Ref. 28) and $ZrN_{0.85}(100)$ (Ref. 26) also indicate that the vacancy-induced states should not show up in normal emission spectra at photon energies below about 30 eV. For substoichiometric VC a vacancy-induced structure was, however, recently observed at 1.8 eV below the Fermi energy in off-normal emission spectra[30] at lower photon energy. Vacancy-induced structures have previously also been identified in angle-integrated photoemission studies of substoichiometric ZrN, TiN,[22,31–34] and NbC,[35] and recent theoretical results[6,7,26–29,36–38] clearly indicate the existence of vacancy-induced states.

The location of peak A is represented by open circles in Fig. 7. This peak does not show any observable dispersion and no pronounced polarization dependence, but it gets more pronounced as the photon energy increases. The main contribution to the intensity seems to originate from indirect transitions, i.e., from a high DOS at the Fermi level. Direct transitions from the uppermost Δ_1 initial-state band should also contribute at the highest photon energies used in Fig. 7, according to the calculated band structure, but they are not possible to distinguish.

At photon energies above 35 eV only one strong peak is observed close to the Fermi energy [see Figs. 4(a) and 5(a)], and this peak probably contains contributions from both the Δ_1 and Δ_5 initial states located close to the Fermi level and from indirect transitions. This peak, and also the vacancy-related peak C, show pronounced intensity modulations with increasing photon energy above 35 eV. In order to visualize the intensity modulations more clearly, the normalized intensity of these peaks are plotted against photon energy in Fig. 8. The peak at the Fermi energy is seen to show a fairly strong resonance behavior with the maximum peak intensity located around 50 eV, and peak C also shows a similar enhancement with the maximum around 48 eV. The shape of these curves and the fact that their maxima coincide fairly well with the maximum in the CFS spectrum suggest that the enhancements originate from resonance photoemission processes of the type discussed above. This implies that the initial states just below the Fermi level are mainly of d character and that the vacancy-induced states should have d character to some extent, in good agreement with the results of a recent partial density-of-states calculation.[7] The resonance effects observed in an earlier study[19] of ZrN also indicated that the vacancy-induced states appear to have an appreciable extent of d character.

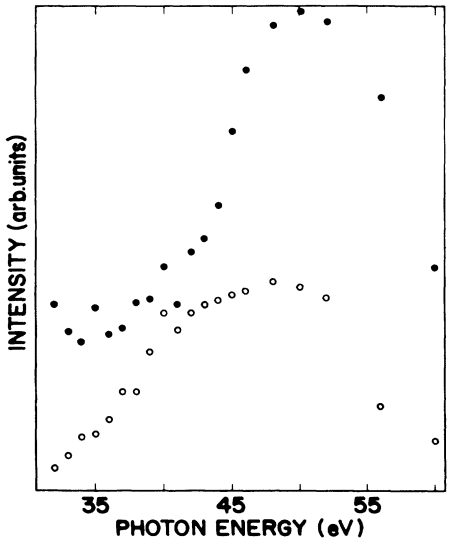

FIG. 8. Variation in emission intensity (peak heights) from states just below the Fermi energy (●) and the vacancy-induced peak (○), obtained from normalized spectra measured at $\theta_i = 45°$. The ratio between the maximum value and the value at 35 eV is 2.4 for the peak at the Fermi energy and 2.8 for the vacancy-induced peak.

SUMMARY

Angle-resolved photoemission experiments performed on a single crystal of $VN_{0.89}(100)$ were presented. The valence-band electronic structure along the Γ–X direction was probed using normal emission spectra and photon energies between 17 and 60 eV. Bulk bands of Δ_1 and Δ_5 symmetry were identified from their polarization dependence. A comparison with theoretical photoemission spectra calculated for stoichiometric composition was made. These spectra, calculated using the bulk potential generated in a LAPW band-structure calculation, were found to reproduce the experimental spectra quite well at photon energies below 35 eV. A mapping of the band structure was made using a fitted free-electron band. The experimentally determined band dispersions were found to be similar but smaller than the theoretical dispersions and the locations of the Δ_5 bands were found to deviate considerably from the theoretically predicted positions.

A structure at -2.8 eV, which had no counterpart in the theoretical spectra, was interpreted as originating from vacancy-induced states. This feature showed no dispersion and a Δ_1-like polarization dependence. A weak resonance behavior of this structure was observed, indicating that the vacancy states have d character, at least to some extent, in agreement with recent calculations[7] made for substoichiometric VN and other TMCN's.

A strong resonance behavior was observed for states located just below the Fermi energy at the V $3p \rightarrow 3d$ absorption resonance, indicating that these states are mainly of d character.

ACKNOWLEDGMENTS

We are grateful to the staff at Daresbury Laboratory for their assistance during the experiments. This work has been supported by the Swedish Natural Science Research Council.

[1]L. E. Toth, *Transition Metal Carbides and Nitrides* (Academic, New York, 1971).
[2]D. A. Papaconstantopoulos, W. E. Pickett, B. M. Klein, and L. L. Boyer, Phys. Rev. B **31**, 752 (1985).
[3]G. Ries and H. Winter, J. Phys. F **10**, 1 (1980).
[4]A. Neckel, P. Rastl, R. Eibler, P. Weinberger, and K. Schwarz, J. Phys. C **9**, 579 (1976).
[5]A. Callenås, L. I. Johansson, A. N. Christensen, K. Schwarz, and P. Blaha, Phys. Rev. B **32**, 575 (1985).
[6]P. Marksteiner, P. Weinberger, A. Neckel, R. Zeller, and P. H. Dederichs, Phys. Rev. B **33**, 812 (1986).
[7]J. Redinger, P. Marksteiner, and P. Weinberger, Z. Phys. B **63**, 321 (1986).
[8]W. K. Schubert, R. N. Shelton, and E. L. Wolf, Phys. Rev. B **23**, 5097 (1981).
[9]A. N. Christensen and P. Roedhammer, J. Cryst. Growth **38**, 281 (1977).
[10]C. Oshima, M. Aono, T. Tanaka, S. Kawai, S. Zaima, and Y. Shibata, Surf. Sci. **102**, 312 (1981).
[11]C. G. Larsson, Ph.D. thesis, Chalmers University of Technology, Gothenburg, 1982.
[12]J. F. L. Hopkinson, J. B. Pendry, and D. J. Titterington, Comput. Phys. Commun. **19**, 69 (1980).
[13]L. I. Johansson, C. G. Larsson, and A. Callenås, J. Phys. F **14**, 1761 (1984).
[14]C. G. Larsson, L. I. Johansson, and A. Callenås, Solid State Commun. **49**, 727 (1984).
[15]R. Haensel, K. Radler, B. Sonntag, and C. Kunz, Solid State Commun. **7**, 1495 (1969).
[16]L. C. Davis, and L. A. Feldkamp, Phys. Rev. Lett. **44**, 673 (1980).
[17]J. A. D. Matthew, and S. M. Girvin, Phys. Rev. B **24**, 2249 (1981).
[18]S. Shin, S. Suga, M. Taniguchi, H. Kanzaki, S. Shibuya, and T. Yamaguchi, J. Phys. Soc. Jpn. **5**, 906 (1982).
[19]J. Lindström, L. I. Johansson, A. Callenås, D. S. L. Law, and A. N. Christensen, Phys. Rev. B **35**, 7891 (1987).
[20]P. A. P. Lindberg, L. I. Johansson, J. Lindström, and D. S. L. Law, Phys. Rev. B **36**, 939 (1987).
[21]P. A. P. Lindberg, L. I. Johansson, J. Lindström, P. E. S. Persson, D. S. L. Law, and A. N. Christensen, Phys. Rev. B, **36**, 6343 (1987).
[22]R. D. Bringans and H. Höchst, Phys. Rev. B **30**, 5416 (1984).
[23]J. Hermanson, Solid State Commun. **22**, 9 (1977).
[24]T.-C. Chiang, J. A. Knapp, M. Aono, and D. E. Eastman, Phys. Rev. B **21**, 3513 (1980).
[25]L. I. Johansson, A. Callenås, P. M. Stefan, A. N. Christensen, and K. Schwarz, Phys. Rev. B **24**, 1883 (1981).
[26]J. Redinger, Solid State Commun. **61**, 133 (1987).
[27]J. Redinger, and P. Weinberger, Phys. Rev. B **35**, 5652 (1987).
[28]J. Redinger, P. Weinberger, and A. Neckel, Phys. Rev. B **35**, 5647 (1987).
[29]W. E. Pickett, B. M. Klein, and R. Zeller, Phys. Rev. B **34**, 2517 (1986).
[30]P. A. P. Lindberg and L. I. Johansson, Z. Phys. B **68**, 83 (1987).
[31]H. Höchst, R. D. Bringans, P. Steiner, and Th. Wolf, Phys. Rev. B **25**, 1783 (1982).
[32]L. Porte, L. Roux, and J. Hanus, Phys. Rev. B **28**, 3214 (1983).
[33]L. Porte, Solid State Commun. **50**, 303 (1984).
[34]E. Beauprez, C. F. Hague, J.-M. Mariot, F. Teyssandier, J. Redinger, P. Marksteiner, and P. Weinberger, Phys. Rev. B **34**, 886 (1986).
[35]H. Höchst, P. Steiner, S. Hüfner, and C. Politis, Z. Phys. B **37**, 27 (1980).
[36]J. Klima, G. Schadler, P. Weinberger, and A. Neckel, J. Phys. F **15**, 1307 (1985).
[37]G. Schadler, P. Weinberger, A. Gonis, and J. Klima, J. Phys. F **15**, 1675 (1985).
[38]J. Redinger, R. Eibler, P. Herzig, A. Neckel, R. Podloucky, and E. Wimmer, J. Phys. Chem. Solids **46**, 383 (1985).